IOPscience iopscience.iop.org

Home Search Collections Journals About Contact us My IOPscience

Sensitivity analysis of periodic errors in heterodyne interferometry

This content has been downloaded from IOPscience. Please scroll down to see the full text.

2011 Meas. Sci. Technol. 22 035305

(http://iopscience.iop.org/0957-0233/22/3/035305)

View the table of contents for this issue, or go to the journal homepage for more

Download details:

IP Address: 152.15.112.62
This content was downloaded on 12/04/2016 at 22:55

Please note that terms and conditions apply.

Meas. Sci. Technol. **22** (2011) 035305 (12pp) doi:10.1088/0957-0233/22/3/035305

Sensitivity analysis of periodic errors in heterodyne interferometry

Vasishta Ganguly, Nam Ho Kim, Hyo Soo Kim and Tony Schmitz[1]

Department of Mechanical and Aerospace Engineering, University of Florida, Gainesville, FL, USA

E-mail: vganguly@ufl.edu, nkim@ufl.edu, hyosoo94@ufl.edu and tschmitz@ufl.edu

Received 16 July 2010, in final form 9 December 2010
Published 4 February 2011
Online at stacks.iop.org/MST/22/035305

Abstract

Periodic errors in heterodyne displacement measuring interferometry occur due to frequency mixing in the interferometer. These nonlinearities are typically characterized as first- and second-order periodic errors which cause a cyclical (non-cumulative) variation in the reported displacement about the true value. This study implements an existing analytical periodic error model in order to identify sensitivities of the first- and second-order periodic errors to the input parameters, including rotational misalignments of the polarizing beam splitter and mixing polarizer, non-orthogonality of the two laser frequencies, ellipticity in the polarizations of the two laser beams, and different transmission coefficients in the polarizing beam splitter. A local sensitivity analysis is first conducted to examine the sensitivities of the periodic errors with respect to each input parameter about the nominal input values. Next, a variance-based approach is used to study the global sensitivities of the periodic errors by calculating the Sobol' sensitivity indices using Monte Carlo simulation. The effect of variation in the input uncertainty on the computed sensitivity indices is examined. It is seen that the first-order periodic error is highly sensitive to non-orthogonality of the two linearly polarized laser frequencies, while the second-order error is most sensitive to the rotational misalignment between the laser beams and the polarizing beam splitter. A particle swarm optimization technique is finally used to predict the possible setup imperfections based on experimentally generated values for periodic errors.

Keywords: interferometry, heterodyne, nonlinearity, periodic, sensitivity

(Some figures in this article are in colour only in the electronic version)

1. Introduction

Heterodyne displacement measuring interferometry offers accurate, high-resolution displacement measurement for non-contact applications. One limitation to the achievable accuracy, however, is the superposition of periodic errors on the measurement signal. These errors are (1) non-cumulative in nature; (2) repeat with each unit wavelength change in the optical path; and (3) depend on misalignments and imperfections in the optical setup, see initial investigations by Quenelle (1983) and Sutton (1987), for example. Apart from periodic errors, there are also other sources of error, such as cosine error, Abbe error, variations in refractive index, thermal deformations, beam shear, non-planar wavefronts, and wavelength instability of the laser source; these are combined into a single uncertainty expression by Schmitz and Kim (2007). While any of these error sources may dominate in a given situation (e.g., uncompensated refractive index changes for measurements in air often limit the displacement measurement accuracy), the purpose of this study is to complete a sensitivity analysis for periodic errors using the analytical model reported by Cosijns *et al* (2002).

A sensitivity analysis is used to study how the uncertainty in model output is related to the uncertainty in the input parameters, see Saltelli *et al* (2008), Saltelli (2002), and Homma and Saltelli (1996). A number of techniques are available. Local sensitivity analysis is based on the derivative of the model output with respect to the input. This gradient approach is inherently local in nature, however, because the

[1] Author to whom any correspondence should be addressed.

 © 2011 IOP Publishing Ltd Printed in the UK & the USA

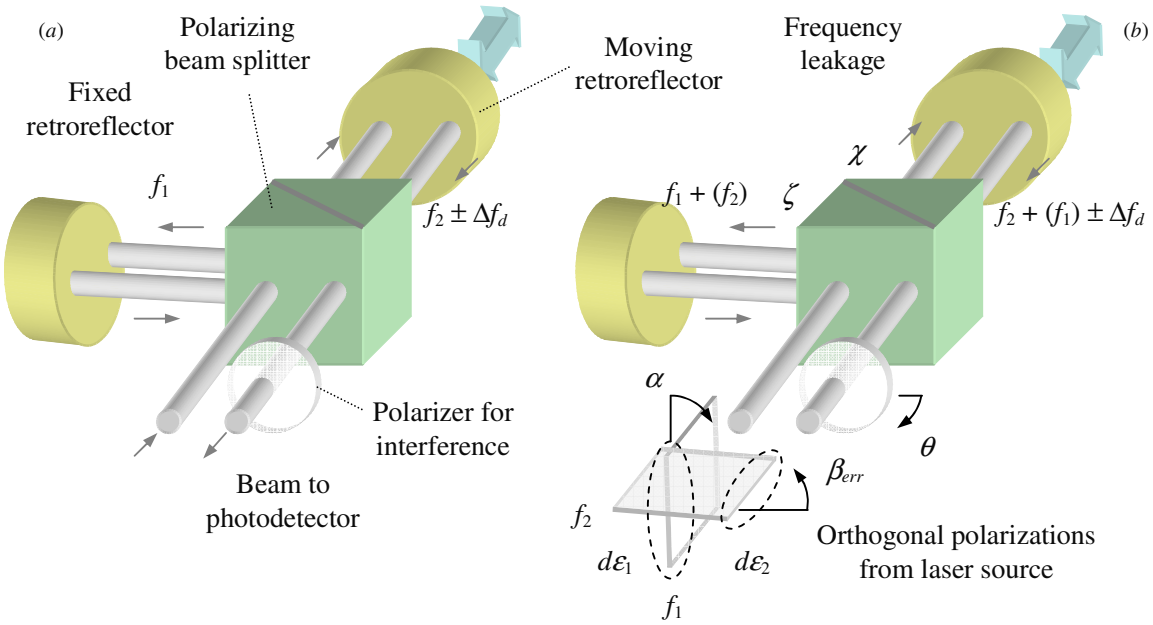

Figure 1. Depictions of (*a*) ideal heterodyne interferometer behavior; and (*b*) frequency leakage (indicated by the frequency terms in parentheses). The two frequencies, f_1 and f_2, are ideally linearly polarized and orthogonal. This enables the polarizing beam splitter to separate them based on their polarization states. The periodic error model terms α, β_{err}, $\text{d}\varepsilon_1$, $\text{d}\varepsilon_2$, θ, ζ, and χ are also identified.

derivative is calculated at a fixed point in the input parameter space. As an alternative, global sensitivity techniques may be applied. Saltelli *et al* (2008) describe variance-based global sensitivity analysis methods which explore the input parameter space by randomly selecting data points from this space and provide a more informative and robust estimate of the behavior of the model output with respect to variation in the model input.

In this study, a variance-based Monte Carlo approach is used to estimate both the individual and total effect Sobol' sensitivity indices for each of the periodic error model inputs using the methods described by Saltelli *et al* (2008), Cukier *et al* (1978), and Sobol' (1993). The study reveals that rotational misalignment of the polarizing beam splitter, the rotational misalignment of the mixing polarizer, and non-orthogonality between the two ideally linearly polarized laser frequencies emitted from the source are the most influential parameters for periodic errors.

Contour plots are provided for a range of uncertainties in linear polarizer (LP) angle, non-orthogonality, and polarizing beam splitter angle to estimate the expected periodic error for a selected combination of uncertainties. A Monte Carlo simulation method is used to evaluate the predicted periodic error for a combination of input uncertainties. Also, a higher order regression fit is applied to the expected periodic error data to provide a closed-form expression for periodic error as a function of the uncertainties in the optical setup. The application of optimization algorithms to estimating setup misalignment errors in order to achieve desired performance levels is also explored. The particle swarm optimization approach described by Kennedy and Eberhart (1998) is used to determine the model input parameters (setup misalignments) given the periodic error data. These results are validated against experimental data and it is shown that the optimization was generally successful in predicting setup misalignments.

2. Periodic error description and measurement

Figure 1 shows a single-pass interferometer setup. For the ideal case (figure 1(*a*)), the two coherent, collinear, orthogonally polarized laser frequencies, f_1 and f_2, are perfectly separated at the polarizing beam splitter and are directed into the reference and measurement arms of the interferometer. Note that a Doppler shift, f_d, occurs for the frequency in the measurement arm during motion. Due to imperfections in the optics or setup (figure 1(*b*)), however, there may be leakage of each frequency into both the measurement and reference arms. This frequency leakage can exist due to non-orthogonality of the two frequencies emitted from the laser source; rotational misalignment of the laser beam with respect to the polarizing beam splitter (PBS); ellipticity of the polarization states; different transmission coefficients for the individual laser beams at the PBS; and rotational misalignment of the polarization axes with respect to the mixing LP. Ghost reflections, nonlinearities in the phase measuring electronics, and beam shear have also been found to induce periodic errors.

Several researchers have reported analytical and numerical models for periodic errors, including Rosenbluth and Bobroff (1990), Bergamin *et al* (1992), Hou and Wilkening (1992), Hou and Zhao (1994), Wu and Su (1996), Wu and Deslattes (1998), Stone and Howard (1998), Schmitz and Beckwith (2003), and Schmitz *et al* (2006). Cosijns *et al* (2002) developed a seven-parameter analytical model for periodic errors which included the rotational misalignment of the input laser beam with respect to the PBS, α; non-orthogonality of the linearly polarized frequencies, β_{err}; ellipticity in the polarizations of the two frequencies, $\text{d}\varepsilon_1$ and $\text{d}\varepsilon_2$; rotational misalignment of the mixing LP (or analyzer), θ; and the two transmission coefficients for the PBS,

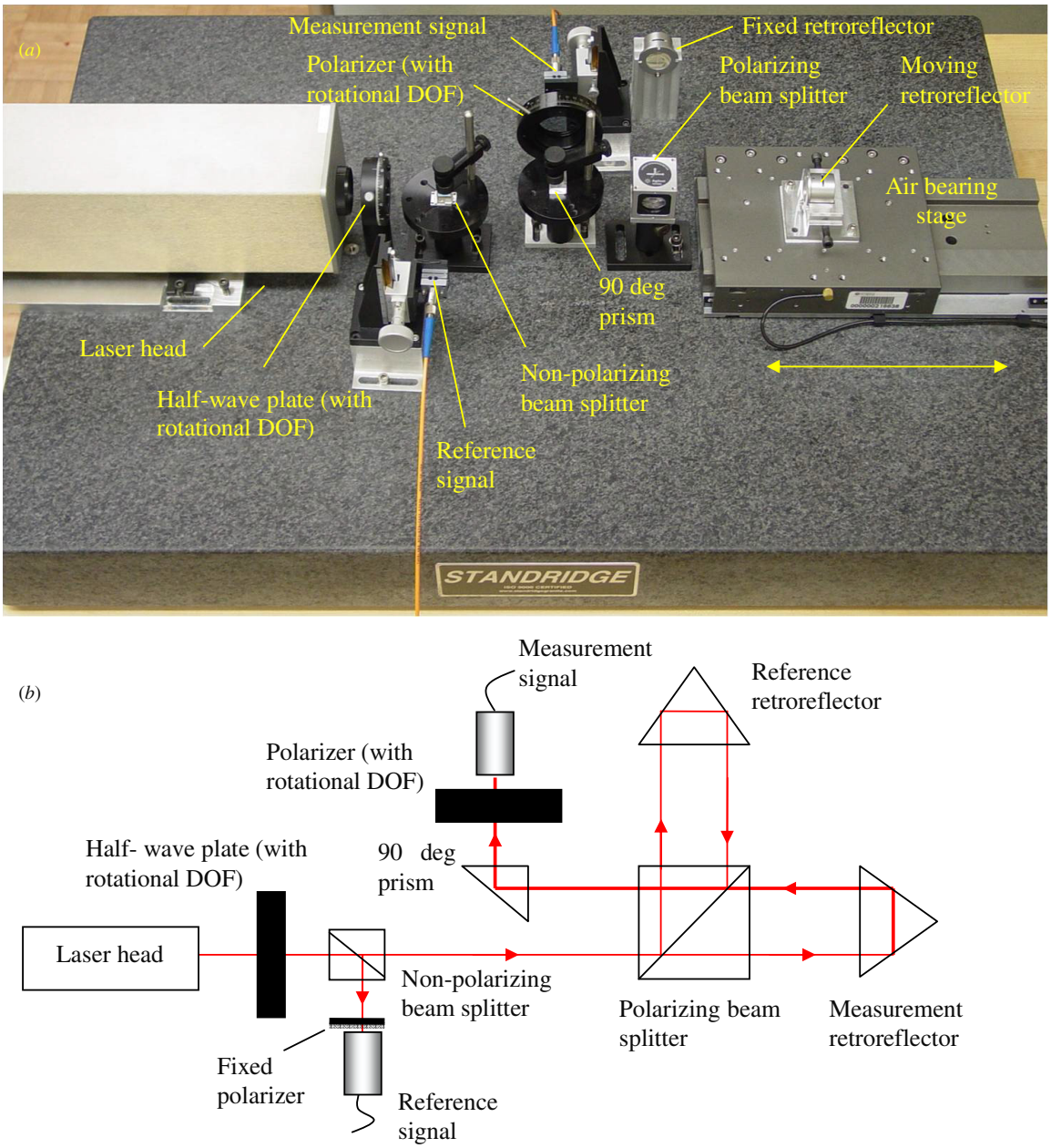

Figure 2. (*a*) Photograph of a single-pass, heterodyne interferometer experimental setup; and (*b*) schematic of a setup. Note that the polarizer and half-wave plate each had a rotational degree of freedom (DOF) about the beam axis to vary the level of periodic error.

ζ and χ. All other parameters were assumed to be ideal. In the work presented here, the Cosijns *et al* (2002) model is used to compute the sensitivity of the periodic error with respect to the seven inputs. (The Cosijns *et al* (2002) model is detailed in the appendix as a convenience to the reader.) In this study, the first- and second-order periodic errors are identified analytically and are summed to obtain the worst-case periodic error. The sensitivity analysis is performed with respect to this sum, as well as the first- and second-order errors independently.

Figure 2 shows the single-pass heterodyne interferometer setup used to verify the Cosijns *et al* (2002) periodic error model. The two-frequency laser head emits the laser beams with nominally orthogonal polarizations that pass through a half-wave plate to a non-polarizing beam splitter (80% transmission/20% reflectance), which splits it into two parts: the reference beam (used as the phase reference in the phase measuring electronics) and the measurement beam (which travels to the interferometer). The reference beam is collected using the reference fiber optic pick-up (which includes a LP oriented at 45° relative to the nominally orthogonal linear polarizations for the two heterodyne frequencies) and forms the reference signal. The measurement beam passes through the PBS where one frequency is (ideally) directed into the reference arm of the interferometer with the stationary retroreflector, while the other frequency is directed into the measurement arm with the moving retroreflector. The frequency in the measurement arm is Doppler-shifted during motion of the moving retroreflector. The two laser beams recombine at the PBS and are directed to the mixing LP.

The interference signal is then collected by the measurement fiber optic pick-up. A half-wave plate is used to artificially vary the rotational misalignment between the two nominally orthogonal, linearly polarized frequencies that make up the source laser beam and the PBS. The orientation of the mixing LP can also be adjusted to vary the periodic error magnitudes. The non-orthogonality of the two frequencies emitted from the laser source, the ellipticities of the two laser beams, and the different transmission coefficients in the PBS are errors inherent in the system and cannot be externally manipulated in this setup[2]. Experiments were carried out for a range of α and θ values, where α was modified using the half-wave plate and θ was varied by the angular orientation of the mixing LP.

3. Sensitivity analysis

Saltelli *et al* (1999) defined sensitivity as: 'The study of how the uncertainty in the output of a model can be apportioned to different sources of uncertainty in model input.' The purpose of this work is to identify which parameters in the single-pass heterodyne interferometer setup are most influential on periodic error by performing a sensitivity analysis. Given this information, efforts in aligning the interferometer may be optimized. An overview of local and global sensitivity analysis methods is provided in the following subsections.

3.1. Local sensitivity analysis

In local sensitivity analysis, the derivative of the model output is computed with respect to the input. The derivative, $\partial Y/\partial X$, of a model output, Y, with respect to an input variable, X, represents the mathematical definition of sensitivity. However, this definition is local in nature because the derivative must be evaluated at a fixed point in the input space; information about the variation is therefore available only at that point. For linear models, the behavior at points far from the evaluation location can be determined by linear extrapolation, but this is not possible for nonlinear problems. Also, local sensitivity methods do not account for the uncertainty in the input variable and are therefore not recommended for models with uncertain inputs. For higher dimensional models with a large number of input parameters, it becomes particularly difficult to compute sensitivities with respect to each variable over the entire range of the input parameter space. However, local sensitivity analysis does provide an initial estimate of those inputs that are most influential on the output.

3.2. Global sensitivity analysis

Although a local, gradient-based sensitivity analysis does provide a measure of the local response of the outputs obtained by individually varying each input, it is ineffective for exploring the entire input parameters space in the case of uncertain inputs. The volume of the space explored is zero because the sensitivity is calculated at a single point with respect to one parameter, while all other parameters are kept constant. In order to obtain better estimates of variation of the outputs over the entire input parameter space, global sensitivity analysis is applied. Variance-based methods enable the computation of output sensitivities given uncertain inputs. These methods compute the output values at a number of points in the input parameter space and use information obtained from a large number of model evaluations to calculate the sensitivity of the output with respect to each input. Global sensitivity measures provide an estimate of how much output variance would be reduced if a particular input parameter was fixed at a certain value. Saltelli *et al* (2008) list selected features of variance-based methods:

- the sensitivity indices are model independent;
- they can capture the full range of input uncertainty;
- they can estimate the individual, as well as interactive, effects of model input on output;
- they can handle inputs which have some logical dependence on each other.

Various techniques have been suggested for sampling individual input parameter sets, including random sampling, Latin hypercube sampling, and quasi-random number generators. This study employs the Latin hypercube sampling method for generating the input parameter dataset. The advantage of Latin hypercube sampling is that it provides improved coverage over the entire input parameter space. Subsequently, it avoids the formation of clusters in the input parameter space which can occur when using random sampling techniques.

Sobol' (2001) described a Monte Carlo method for computing global sensitivity indices of arbitrary groups of factors. The individual effect of an input is defined as the reduction in output variance when the input is fixed at a certain value. The sensitivity index, S_i, is defined in terms of the unconditional variance of the output, $V(Y)$, and the variance in the output Y when the input parameter, X_i, is fixed, $V\,[E\,(Y|\,X_i)]$:

$$S_i = \frac{V\,[E\,(Y|\,X_i)]}{V\,(Y)}. \tag{1}$$

This index represents the primary (first order) effect of X_i on Y without taking into consideration interaction effects. These individual effect sensitivity indices identify which parameters most influence output variation and can be used in a factor prioritization setting.

The total effect sensitivity index takes into consideration the interactive effects of the various input parameters on output variance. The total effect sensitivity index, ST_i, shown in (2) is expressed in terms of $V(Y)$ and the output variance $V\,[E\,(Y|\,X_{\sim i})]$, which is the variance computed when all parameters except X_i are fixed. The total effect sensitivity indices can be used in a factor fixing setting. If ST_i is approximately zero, then X_i can be fixed at any value within its input range without affecting the output variance:

$$\mathrm{ST}_i = 1 - \frac{V\,[E\,(Y|\,X_{\sim i})]}{V\,(Y)}. \tag{2}$$

A Monte Carlo approach was used here to compute the Sobol' sensitivity indices, where larger sample sizes yield an

[2] These error sources were not quantified, but were assumed to remain constant for all experiments.

increased accuracy of the results. The step-by-step procedure adopted to calculate the sensitivity indices follows.

First, the two $N \times k$ matrices, A and B, were defined as shown in (3) using a Latin hypercube sampling technique, where N is the number of samples and k is the number of input parameters ($k = 7$ in this case). The column of each matrix corresponds to a selected input parameter (identified by the subscript) with random values within its input uncertainty range (the sample number is indicated by the superscript). Note that A and B are generated independently and are separate matrices:

$$A, B = \begin{bmatrix} x_1^1 & x_2^1 & \cdots & x_{k-1}^1 & x_k^1 \\ x_1^2 & x_2^2 & \cdots & x_{k-1}^2 & x_k^2 \\ \vdots & \vdots & \ddots & \vdots & \vdots \\ x_1^{N-1} & x_2^{N-1} & \cdots & x_{k-1}^{N-1} & x_k^{N-1} \\ x_1^N & x_2^N & \cdots & x_{k-1}^N & x_k^N \end{bmatrix}. \tag{3}$$

Second, a C_i matrix ($i = 1$ to k) was defined as shown in (4) for each input parameter by replacing the ith column of the B matrix with the ith column of the A matrix:

$$C_i = \begin{bmatrix} x_{1B}^1 & x_{2B}^1 & \cdots & x_{iA}^1 & \cdots & x_{k-1B}^1 & x_{kB}^1 \\ x_{1B}^2 & x_{2B}^2 & \cdots & x_{iA}^2 & \cdots & x_{k-1B}^2 & x_{kB}^2 \\ \vdots & \vdots & \ddots & \vdots & \ddots & \vdots & \vdots \\ x_{1B}^{N-1} & x_{2B}^{N-1} & \cdots & x_{iA}^{N-1} & \cdots & x_{k-1B}^{N-1} & x_{kB}^{N-1} \\ x_{1B}^N & x_{2B}^N & \cdots & x_{iA}^N & \cdots & x_{k-1B}^N & x_{kB}^N \end{bmatrix}. \tag{4}$$

Third, the model output was computed using input samples from the A, B, and C_i matrices as shown in (5). This generates the output vectors, where each row of the A, B, and C_i matrices forms a single input data point. Finally, the individual effect and total effect sensitivity indices were defined as shown in (6) and (7), respectively:

$$y_A = \begin{bmatrix} f\left(A^1\right) \\ f\left(A^2\right) \\ \vdots \\ f\left(A^{N-1}\right) \\ f\left(A^N\right) \end{bmatrix} \qquad y_B = \begin{bmatrix} f\left(B^1\right) \\ f\left(B^2\right) \\ \vdots \\ f\left(B^{N-1}\right) \\ f\left(B^N\right) \end{bmatrix}$$

$$y_{C_i} = \begin{bmatrix} f\left(C_i^1\right) \\ f\left(C_i^2\right) \\ \vdots \\ f\left(C_i^{N-1}\right) \\ f\left(C_i^N\right) \end{bmatrix} \tag{5}$$

$$S_i = \frac{\frac{1}{N}\sum_{j=1}^{N} y_A^j y_{C_i}^j - f_0^2}{\frac{1}{N}\sum_{j=1}^{N}\left(y_A^j\right)^2 - f_0^2}, \quad \text{where} \quad f_0^2 = \left(\frac{1}{N}\sum_{j=1}^{N} y_A^j\right)^2 \tag{6}$$

$$\mathrm{ST}_i = \frac{\frac{1}{N}\sum_{j=1}^{N} y_B^j y_{C_i}^j - f_0^2}{\frac{1}{N}\sum_{j=1}^{N}\left(y_A^j\right)^2 - f_0^2}. \tag{7}$$

Once the Sobol' sensitivity indices are calculated, their values must be interpreted. The index S_i is a measure of how much the output variance can be reduced by fixing X_i. It is independent of the interactive effects or the total effect sensitivity indices. The total effect index ST_i is greater than S_i in the presence of interactive effects; it is equal to S_i when there are no interactive effects. The difference between ST_i and S_i is a measure of the interactive effects for a particular parameter. If ST_i is zero (S_i is also equal to zero), this indicates that a particular parameter has no influence on the output and can be fixed at any value within its input uncertainty range. The sum of all S_i indices is equal to 1 for models with no interactive effects (additive models) and is less than 1 for models with interactive effects (non-additive models). The difference $1 - \sum_{i=1}^{k} S_i$ is an indicator of how significant interactive effects are in the model. The sum of all ST_i should be greater than 1 in general and is equal to 1 for additive models.

4. Predicting periodic error from input uncertainty

A first objective of this study was to predict the expected periodic error magnitude based on the input uncertainties for a particular heterodyne interferometer setup. As noted previously, the Cosijns *et al* (2002) model was implemented to complete this activity. This section describes the procedure and the results are provided in section 6. As shown in section 6, the most important parameters in the Cosijns *et al* (2002) model were determined to be α, θ, and β_{err} based on a global sensitivity analysis. The expected value of periodic error for a given combination of setup uncertainties (in these values) was then determined using Monte Carlo simulation. The expected value of periodic error was considered to be the value below which 95% (approximately two standard deviations, or 2σ) of the periodic error values computed by the Monte Carlo simulation occurred (a sample size of 2000 was used).

The expected periodic error was computed for a complete array of uncertainties in the rotational misalignment of the PBS, rotational misalignment of the mixing LP, and non-orthogonality of the two frequencies. The uncertainties in the ellipticities and transmission coefficients were kept constant due to their low sensitivity. Contour plots are provided for different values for uncertainty in the mixing polarizer orientation.

From the simulation data, a regression fit with higher order terms was then completed in order to obtain an expression for the expected value of periodic error, pe (the sum of first- and second-order contributions, considered as a worse case scenario). A satisfactory fit was obtained with the inclusion of cubic terms. The expression is of the form shown in (8), where the b terms are the regression coefficients, $k = 3$ is the number of variables (α, θ, and β_{err} for the simplified model), and x specifies the uncertainties in α, θ, and β_{err}. This expression provides an estimate of the expected value of periodic error given uncertainties in the setup misalignments. The expression does not incorporate variation in the uncertainties in the beam ellipticities, $\mathrm{d}\varepsilon_1$ and $\mathrm{d}\varepsilon_2$, or the transmission coefficients,

ξ and χ; their uncertainties were assumed to be constant:

$$pe = b_0 + \sum_{p=1}^{k} b_p x_p + \sum_{p=1}^{k}\sum_{q=p}^{k} b_{pq} x_p x_q + \sum_{p=1}^{k}\sum_{q=p}^{k}\sum_{r=q}^{k} b_{pqr} x_p x_q x_r. \quad (8)$$

5. Predicting interferometer setup misalignments

The second objective of this study was to predict the setup misalignments based on the measured periodic error. The approach is described here and results are provided in section 6. Corrective measures can then be taken to reduce these errors. An optimization problem was solved to find the setup misalignments which would produce the same periodic error as the measured error. The objective function of the optimization problem was defined to minimize the difference between the periodic error measured using the phase measuring electronics and the periodic error predicted using the Cosijns *et al* (2002) model using the setup misalignment values of the candidate solution. The objective function was

$$\text{minimize } f = (\text{FO}_m - \text{FO}_c)^2 + (\text{SO}_m - \text{SO}_c)^2, \quad (9)$$

where FO_m and SO_m are the measured first- and second-order periodic errors and FO_c and SO_c are the candidate periodic errors computed using the Cosijns *et al* (2002) model. A particle swarm optimization (PSO) technique was used to solve the optimization problem. In PSO, a swarm of candidate individuals are initialized in the design space. The value of the objective function is calculated and the best individual in the swarm is identified. The velocity vector, V_i, for each step in the optimization consists of four terms: the inertia term, the neighborhood term (subscript n), the global term (subscript g), and the personal term (subscript p). In (10), the C terms are coefficients which determine the weight of each parameter (i.e. their contribution to the velocity), the R terms are random numbers, w is the inertia weight, V_{i-1} is the velocity in the previous step, X_n is the position of the neighborhood best particle, X_g is the position of the global best particle, X_p is the position of the personal best particle, and X_i is the current position. The new position of the particle is computed using (11):

$$V_i = wV_{i-1} + C_n R_n(X_n - X_i) + C_g R_g(X_g - X_i) + C_p R_p(X_p - X_i) \quad (10)$$

$$X_{i+1} = X_i + V_i. \quad (11)$$

The inertia weight controls the influence of the previous velocity on the new velocity. A large inertia weight facilitates greater exploration by encouraging the new search areas in the design space; this gives the optimization process its global nature. The inertia weight is typically reduced linearly in each iteration until it reaches zero. The neighborhood weight makes use of the intelligence of particles in the local neighborhood in determining the velocity vector. The neighborhood term is not always included in standard PSO algorithms. The global weight determines how much influence the global best particle has on the velocity vector, while the personal weight determines how much the velocity vector of a particle depends on its personal best. In this study the velocity equation was truncated to include only the global and personal terms. It was found through trial and error that the inertia term, wV_{i-1}, and the neighborhood component, $C_n R_n(X_n - X_i)$, did not contribute to improving the result or increasing computational efficiency and they were therefore not considered. The results obtained using only the personal and global weights were found to be sufficiently robust.

The optimization was initially performed taking into consideration all seven variables/setup parameters in the Cosijns *et al* (2002) model. However, in most interferometer setups, only the rotational alignment of the laser beam and PBS and the rotational alignment of the mixing LP are controlled, while the other parameters depend on component manufacturing and cannot be changed *in situ*. The optimization algorithm was therefore modified to consider only these two parameters. It was observed that most periodic errors can be corrected by varying only these two parameters. Figure 3 shows an example of the optimization process where the swarm is plotted at different stages with arrows indicating the velocity components. Black dots indicate particles that are closest to the optimum solution, while white dots indicate particles that are furthest away (the arrows show the velocity). The migration toward the α and θ combination in the 50th iteration identifies the parameter combination that yields the measured first- and second-order periodic errors. For figure 3, the optimization was performed with target first- and second-order errors of 10 nm each. From the optimization process, a combination of $\alpha = 22.9^\circ$ and $\theta = 6.6^\circ$ was obtained which would produce this combination of periodic errors.

The optimization problem was applied to the experimental periodic error data obtained over a range of α and θ values. The error magnitudes are supplied to the PSO algorithm and the α and θ values were compared to those used in the experimental setup. Also, as a check for the optimization accuracy, periodic errors were computed for a range of α and θ values using the Cosijns *et al* (2002) model. This periodic error data was then input to the PSO algorithm and the α and θ values obtained from the algorithm were compared to the original α and θ values used in the model to compute periodic error.

6. Results

6.1. Experimental verification of the periodic error model

Experiments were carried out with the moving retroreflector (mounted on the air bearing stage) commanded to translate with a velocity of 50 mm min^{-1}, while position data were collected at a sampling frequency of 312.5 kHz. To determine the periodic error, a polynomial fit was first extracted from the position data to isolate the (residual) periodic error from the macro-scale position data. The discrete Fourier transform of the position data was then performed. From this result, the first- and second-order periodic error magnitudes were identified based on their frequency. These magnitudes were compared with analytical values computed using the Cosijns

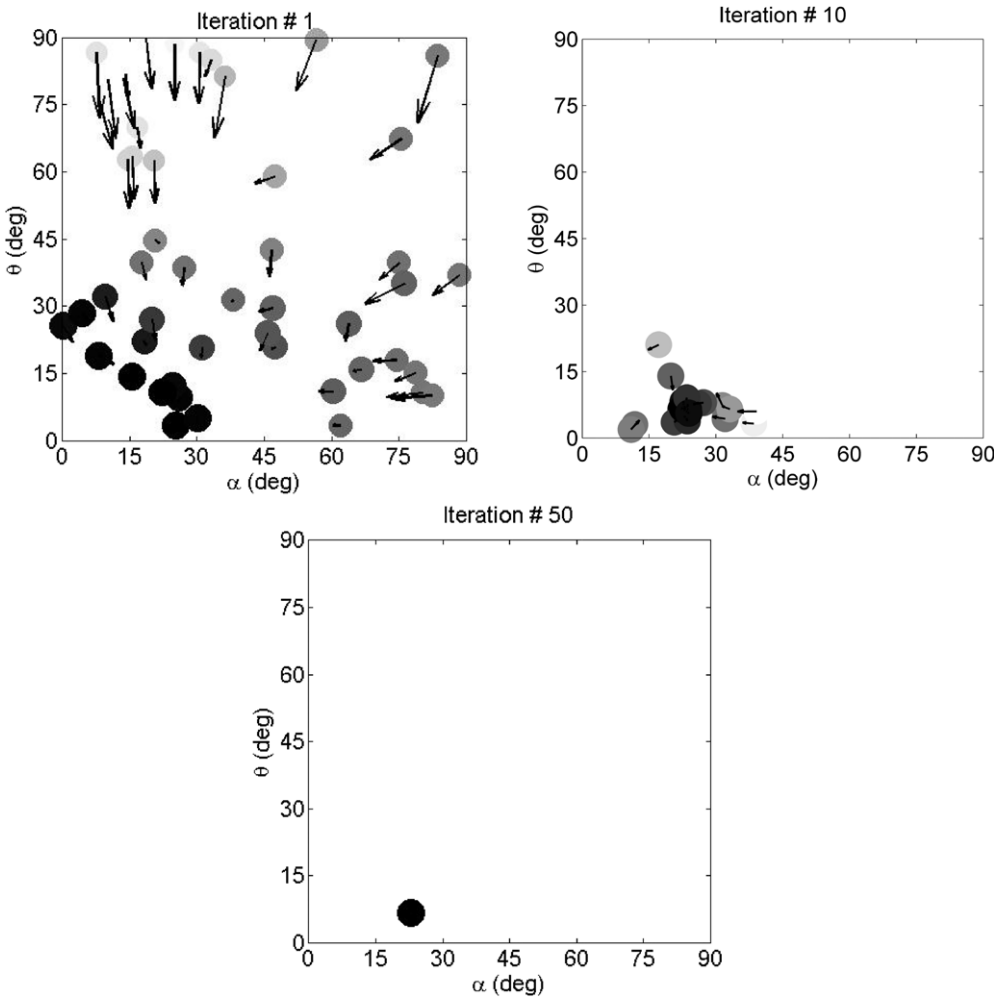

Figure 3. Example particle swarm optimization process; results for the 1st, 10th, and 50th iterations are provided.

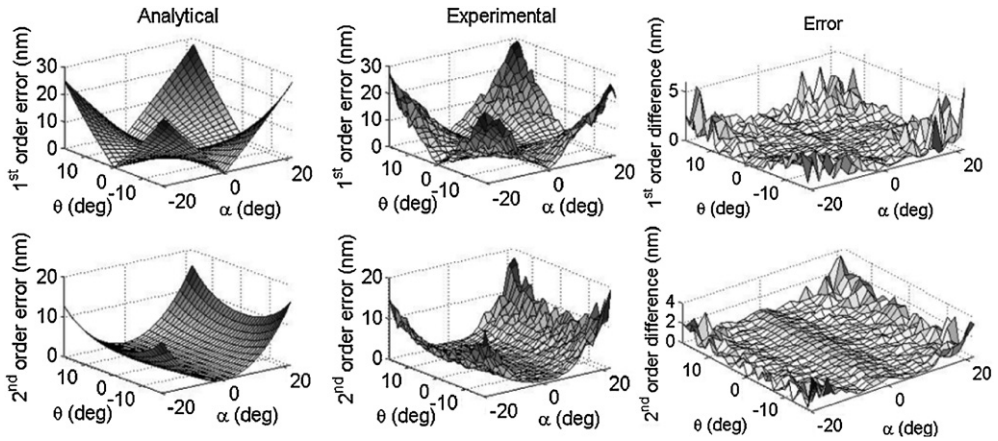

Figure 4. First-order (top) and second-order (bottom) periodic errors; analytical (left) and experimental (middle) results are included. The differences between the analytical and experimental results are also included (right).

et al (2002) model for a range of α and θ values ($\pm 20^{\circ}$). The angle α was set by the orientation of the half-wave plate, while θ was varied by changing the mixing LP angle. Figure 4 shows the comparison of experimental results and model predictions for the first- and second-order periodic errors; they are found to be in good agreement with each other except for very large misalignments. Figure 4 also displays the differences between the experimental and predicted results.

The differences in figure 4 can be explained by the uncertainties in the optical setup parameters. For any given combination of α and θ, a new periodic error estimate can be computed taking setup uncertainties into account as described

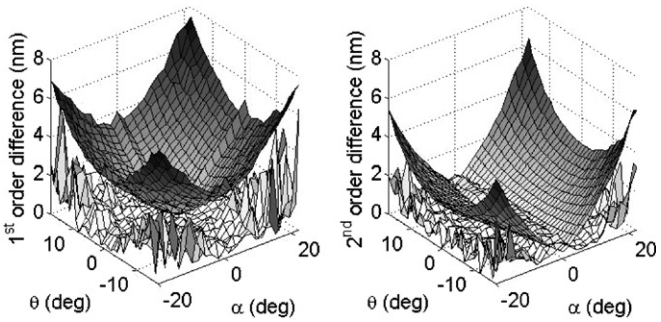

Figure 5. Differences between the experimental and predicted first-order (left) and second-order (right) periodic errors, including the upper limits (top surface) obtained by considering uncertainty.

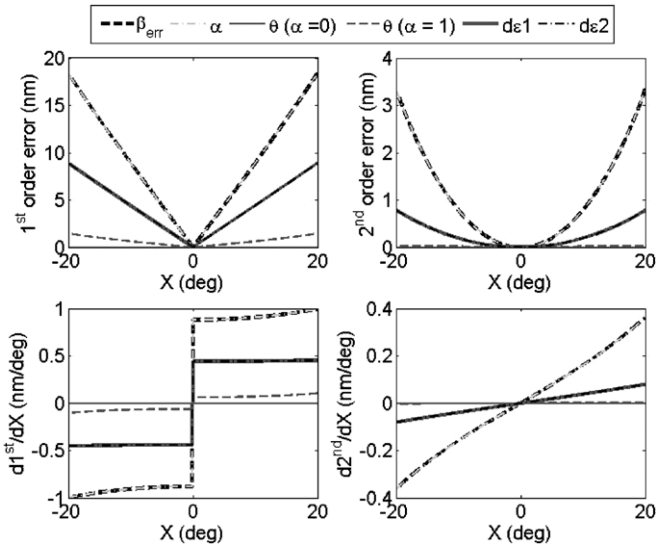

Figure 6. Local sensitivity for the first-order (left) and second-order (right) periodic errors with respect to α, β_{err}, θ, $\mathrm{d}\varepsilon_1$, and $\mathrm{d}\varepsilon_2$. The top plots show periodic errors and the bottom plots show sensitivities.

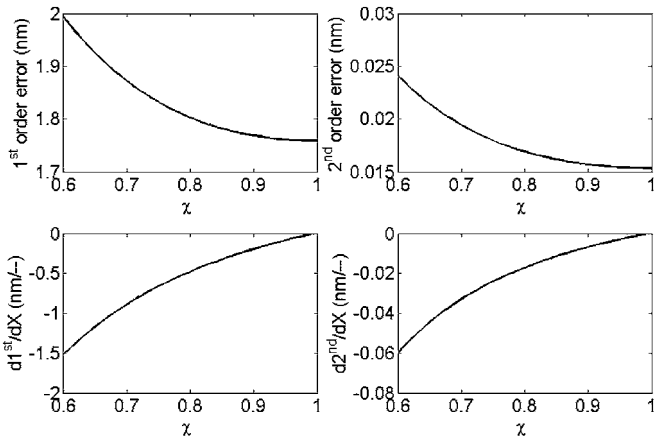

Figure 7. Local sensitivity for the first-order (left) and second-order (right) periodic errors with respect to χ. The top plots show periodic errors and the bottom plots show sensitivities.

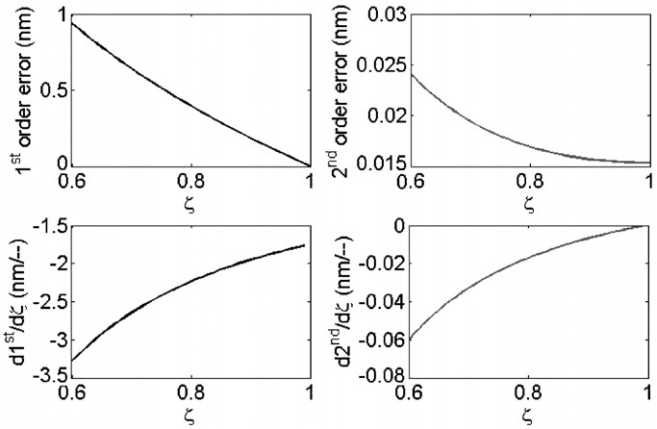

Figure 8. Local sensitivity for the first-order (left) and second-order (right) periodic errors with respect to ζ. The top plots show periodic errors and the bottom plots show sensitivities.

in section 4. Thus, upper limits for periodic error can be estimated by considering the input uncertainties. It is seen in figure 5 that the differences between the analytical and the experimental periodic errors are accounted for when including setup uncertainty.

6.2. *Sensitivity analysis*

6.2.1. Local sensitivity. Local sensitivities for the first- and second-order periodic errors were computed with respect to each of the setup parameters, independently while all the other parameters were maintained at their nominal values. Figure 6 shows the sensitivities with respect to the rotational misalignment between the laser beam and PBS, α, the non-orthogonality of the two laser beams, β_{err}, the rotational misalignment of the mixing LP, θ, and the two polarization ellipticities, $\mathrm{d}\varepsilon_1$ and $\mathrm{d}\varepsilon_2$. Figures 7 and 8 show sensitivities with respect to the transmission coefficients, χ and ζ. The misalignment of the LP and the PBS transmission coefficients have no effect on periodic error when all the other parameters are maintained at their nominal values. Therefore, the sensitivities of these parameters were computed with $\alpha = 1^\circ$. From the figures it is observed that both first- and second-order errors are most influenced by α and β_{err} (which overlap in figure 7). Local sensitivity, however, provides no indication of the interactive effects between different variables. A global sensitivity analysis was therefore also completed.

6.2.2. Sobol' sensitivity indices. The Sobol' individual effect and total effect sensitivity indices were computed using the Monte Carlo approach described previously with a sample size of 1×10^6. The input parameter uncertainty ranges used in the analysis are listed in table 1 (normal distributions were assumed).

Table 2 shows the individual effect, total effect, and interactive effect sensitivity indices computed for the sum of the first- and second-order periodic errors as a worse case scenario, as well as for consideration of first- and second-order errors independently. As seen from the results for the given input range, periodic order error is mainly dominated by β_{err}. However, the total sensitivity indices for α and θ are also significant, indicating that their interactive effects with

Table 1. Uncertainty ranges for input parameters.

Parameter	Uncertainty range (3σ)
α	5°
θ	5°
$d\varepsilon_1$	1°
$d\varepsilon_2$	1°
ζ	0.05
χ	0.05
β_{err}	1°

other parameters are important. The angular orientations α, θ, and β_{err} are the main interacting parameters. The polarization ellipticities, $d\varepsilon_1$ and $d\varepsilon_2$, and the transmission coefficients, ζ and χ, have little influence. Other simulations conducted with different input uncertainty values produced similar results. Also, the second-order periodic error depends primarily on α.

6.3. Periodic error prediction

The expected values of periodic errors were computed for an array of input uncertainties: $\alpha = 0°$ to 5°, $\theta = 0°$ to 5°, and $\beta_{err} = 0°$ to 1°. The lines of the constant periodic error (the sum of the first- and second-order errors in nm) were plotted in the α–β_{err} plane for different values of θ uncertainty. From these contour plots, the expected value of periodic error can be identified for a given combination of input parameter uncertainties. The uncertainty in the ellipticities was fixed at 1° and the transmission coefficient uncertainties were both 0.05. Figures 9 and 10 show results for θ uncertainties of 5° and 2°, respectively. Using these figures, a regression fit (with higher order terms) to the expected periodic error sum, pe, was completed. The fit is shown in (12), where insignificant terms have been eliminated. Note that the α, θ, and β_{err} terms are the 3σ normally distributed uncertainties. This equation can be used to estimate the expected periodic error given uncertainties in α, θ, and β_{err} for any single pass heterodyne interferometer setup:

$$pe = 0.4115 + 0.2807\beta_{err}^2 + 0.0011\alpha^2\theta + 0.0009\alpha\theta^2 - 0.0048\alpha\theta - 0.0788\beta_{err} + 0.0182\alpha\beta_{err} + 0.0005\alpha^3 - 0.0092\alpha\beta_{err}^2. \quad (12)$$

6.4. Setup misalignments prediction

Based on knowledge of the first- and second-order periodic error magnitudes, the Cosijns *et al* (2002) model was applied to compute the values of the corresponding interferometer setup misalignments using the PSO approach described previously. Given these predicted misalignments, corrective measures can be applied to reduce the error. The optimization was performed with periodic errors obtained both experimentally and analytically for a wide range of α and θ values to determine if the optimization algorithm returned the appropriate α and θ values in both instances.

The α and θ values obtained from the optimization process were plotted as three-dimensional (3D) surfaces. A 3D surface

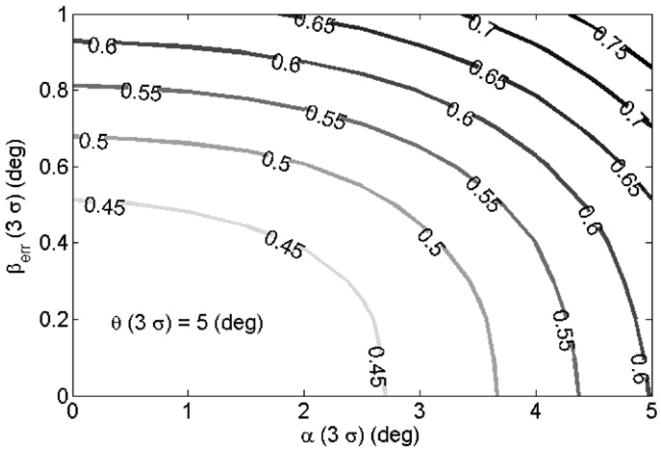

Figure 9. Contour plot for the expected periodic error sum ($\theta = 5°$).

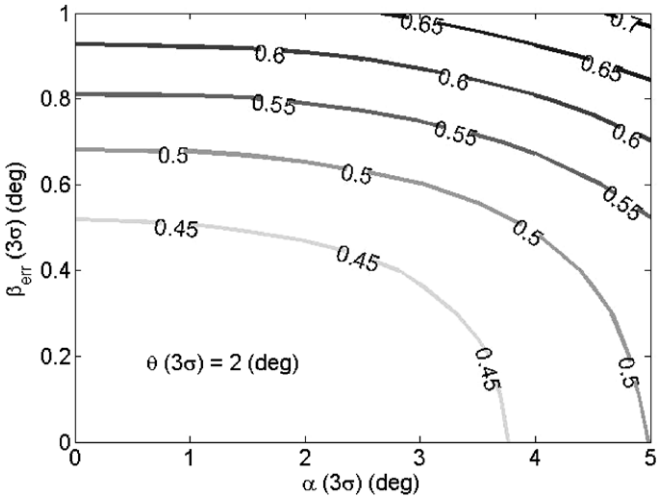

Figure 10. Contour plot for the expected periodic error sum ($\theta = 2°$).

Table 2. Sobol' sensitivity indices (important indices are indicated using a bold font).

	Individual effect S_i			Total effect ST_i			Interactive effect $ST_i - S_i$		
	FO + SO	FO	SO	FO + SO	FO	SO	FO + SO	FO	SO
α	**0.202**	0.038	**0.979**	**0.462**	**0.348**	**0.999**	**0.260**	**0.310**	0.020
θ	0.034	0.040	0.001	**0.284**	**0.341**	0.002	**0.250**	**0.301**	0.001
$d\varepsilon_1$	0.034	0.041	0.001	0.114	0.141	0.002	0.080	0.099	0.001
$d\varepsilon_2$	0.035	0.041	0.001	0.115	0.141	0.002	0.080	0.100	0.001
ζ	0.002	0.001	0.001	0.013	0.015	0.002	0.011	0.014	0.001
χ	0.002	0.001	0.001	0.012	0.014	0.002	0.011	0.013	0.001
β_{err}	**0.349**	**0.421**	0.001	**0.581**	**0.697**	0.021	**0.231**	**0.276**	0.020

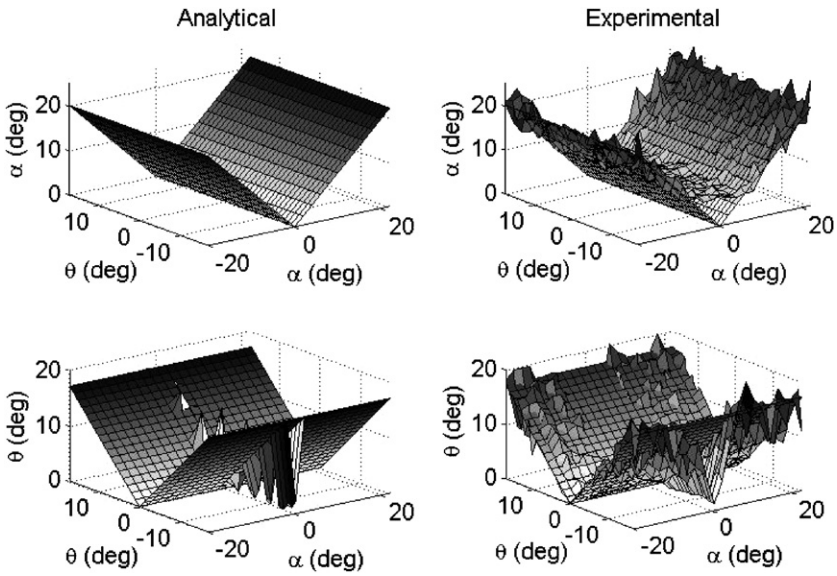

Figure 11. PSO results with periodic error input: (left) analytical periodic error data; (right) experimental periodic error data.

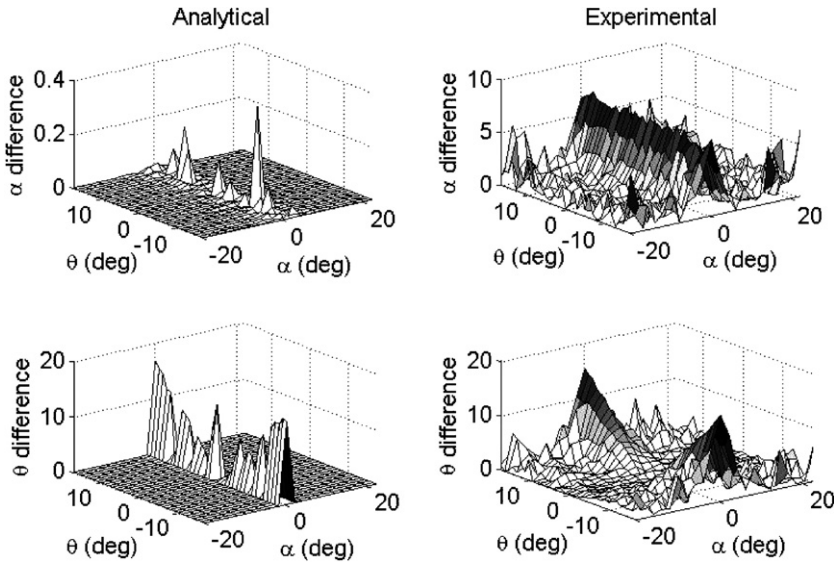

Figure 12. Differences between PSO algorithm results and input α and θ values based on periodic error: (left) analytical periodic error data; (right) experimental periodic error data.

of the true values for α and θ (i.e., the input α and θ values for the analytical results and setup α and θ values for experimental results) was also included as an overlapping layer. From figure 11 it is seen that the output α and θ values obtained from the PSO algorithm match closely with the analytical input data values. Although similar trends are observed for the experimental data, the results are not as closely matched. Figure 12 shows the difference between the input α and θ values and the values obtained from the optimization algorithm for both analytical and experimental data.

For the analytical data, large differences in θ are observed when α is zero. This is because θ does not have any independent effect on periodic error in the model and only acts in combination with α. Thus, when α is equal to zero, θ is free to take up any value without affecting the output; the result is large errors in predicting θ values in this specific case. The differences in α are small. Experimental results show significant differences in both α and θ for low α. These can be attributed to uncertainty in the periodic error data itself (figure 4). Ideally, for low α and θ values, the periodic error should be close to zero. However, the input α and θ settings for the experimental data are subject to their own uncertainties. From table 2, it is seen that the second-order periodic error is highly sensitive to α. Therefore, during the optimization process where α and θ values are being estimated from the measured periodic error the opposite holds true, i.e. the α value is highly sensitive to the second-order periodic error level. Since some periodic errors are always present due to measurement limitations, it is propagated to high estimated values of α and, therefore, large errors during the optimization process.

7. Conclusions

In this work, sensitivity analyses were completed for periodic errors in heterodyne displacement measuring interferometry. The initial local sensitivity analysis showed that periodic error depends mostly on variations in the misalignment about the optical axis between the laser head polarizations and the interferometer's polarizing beam splitter, α, and non-orthogonality between the two linearly polarized frequencies emitted from the laser head, β_{err}. The Sobol' global sensitivity index method was then used to evaluate individual and total effect sensitivity indices. The sensitivity indices obtained from this analysis suggested that periodic error depends mainly on α, β_{err}, and the angular misalignment of the mixing LP for the interferometer, θ. Only β_{err} showed a significant individual effect; however, α and θ were shown to interact with each other, as well as with β_{err}, and significantly affect periodic error. This suggests that, in order to restrict periodic error to a low value, the rotational alignment of the laser head with the PBS and the rotational alignment of the mixing LP must be accurate. Also, a laser source with orthogonal (linearly polarized) frequencies must be selected. Using a Monte Carlo simulation approach, the expected periodic error for input uncertainties was determined and contour plots were developed. Based on these results, a regression fit was completed to obtain a closed-form expression that can be used to predict periodic error given the uncertainties in the optical setup. This could be used to evaluate the applicability of a commercial system to a particular measurement application (based on the manufacturer-specified uncertainty in the beam orthogonality, for example).

The use of an optimization algorithm as a predictive tool in estimating α and θ errors based on the measured periodic error magnitudes was also investigated. The periodic error obtained from the phase measuring electronics was used to find corresponding setup imperfections. Although this method does show some promise, it fails for low values of α due to model limitations (e.g., ghost reflections, beam shear, and nonlinearities in the phase measuring electronics were not considered) and uncertainties associated with periodic error measurements.

Acknowledgments

This work was supported by the National Science Foundation (DMI-0555645) and Agilent Technologies, Inc. Any opinions, findings, and conclusions or recommendations expressed in this material are those of the authors and do not necessarily reflect the views of these agencies.

Appendix

The Cosijns *et al* (2002) analysis propagates: ellipticity of the two (nominally linear) polarizations; non-orthogonality between the two polarizations; rotation of the polarization axes relative to the polarizing beam splitter (which ideally separates the coincident frequencies into the measurement and reference paths); transmission coefficient variations for the polarizing beam splitter; and rotation of the mixing LP, which causes interference of the measurement and reference beams, relative to its nominal 45° orientation (for vertical and horizontal source polarizations) through the interference equations to arrive an expression for the periodic phase error, $\Delta\phi_{pe}$. See (A.1), where θ is the deviation of the polarizer angle from 45° and the variables A–F are defined in (A.2)–(A.7).

$$\Delta\phi_{pe} = -\tan^{-1}\left(\frac{A + B\sin(2\theta) + C\cos(2\theta)}{D + E\sin(2\theta) + F\cos(2\theta)}\right) \tag{A.1}$$

$$\begin{aligned} A = {} & (-(\zeta^2\sin(\beta)^2 + \chi^2\cos(\beta)^2)\cos(\mathrm{d}\varepsilon_1/2)\sin(\mathrm{d}\varepsilon_2/2) \\ & -(\zeta^2\cos(\alpha)^2 + \chi^2\sin(\alpha)^2)\sin(\mathrm{d}\varepsilon_1/2) \\ & \cos(\mathrm{d}\varepsilon_2/2))\cos(\Delta\phi) + (\zeta^2\cos(\alpha)\sin(\beta) \\ & +\chi^2\sin(\alpha)\cos(\beta))\cos(\mathrm{d}\varepsilon_1/2 + \mathrm{d}\varepsilon_2/2)\sin(\Delta\phi) \end{aligned} \tag{A.2}$$

$$\begin{aligned} B = {} & ((\zeta^2\sin(\beta)^2 - \chi^2\cos(\beta)^2)\cos(\mathrm{d}\varepsilon_1/2)\sin(\mathrm{d}\varepsilon_2/2) \\ & +(\zeta^2\cos(\alpha)^2 - \chi^2\sin(\alpha)^2)\sin(\mathrm{d}\varepsilon_1/2) \\ & \cos(\mathrm{d}\varepsilon_2/2))\cos(\Delta\phi) + (-\zeta^2\cos(\alpha)\sin(\beta) \\ & +\chi^2\sin(\alpha)\cos(\beta))\cos(\mathrm{d}\varepsilon_1/2 + \mathrm{d}\varepsilon_2/2)\sin(\Delta\phi) \end{aligned} \tag{A.3}$$

$$\begin{aligned} C = {} & \zeta\chi(\cos(\beta)\sin(\beta)\cos(\mathrm{d}\varepsilon_1/2)\sin(\mathrm{d}\varepsilon_2/2)(1 - \cos(2\Delta\phi)) \\ & +\sin(\alpha)\sin(\beta)\cos(\mathrm{d}\varepsilon_1/2)\cos(\mathrm{d}\varepsilon_2/2)\sin(2\Delta\phi) \\ & -\cos(\alpha)\cos(\beta)\sin(\mathrm{d}\varepsilon_1/2)\sin(\mathrm{d}\varepsilon_2/2)\sin(2\Delta\phi) \\ & -\sin(\alpha)\cos(\alpha)\sin(\mathrm{d}\varepsilon_1/2)\cos(\mathrm{d}\varepsilon_2/2)(1 + \cos(2\Delta\phi))) \end{aligned} \tag{A.4}$$

$$\begin{aligned} D = {} & ((\zeta^2\sin(\beta)^2 + \chi^2\cos(\beta)^2)\cos(\mathrm{d}\varepsilon_1/2)\sin(\mathrm{d}\varepsilon_2/2) \\ & +(\zeta^2\cos(\alpha)^2 + \chi^2\sin(\alpha)^2)\sin(\mathrm{d}\varepsilon_1/2) \\ & \cos(\mathrm{d}\varepsilon_2/2))\sin(\Delta\phi) + (\zeta^2\cos(\alpha)\sin(\beta) \\ & +\chi^2\sin(\alpha)\cos(\beta))\cos(\mathrm{d}\varepsilon_1/2 + \mathrm{d}\varepsilon_2/2)\cos(\Delta\phi) \end{aligned} \tag{A.5}$$

$$\begin{aligned} E = {} & ((-\zeta^2\sin(\beta)^2 + \chi^2\cos(\beta)^2)\cos(\mathrm{d}\varepsilon_1/2)\sin(\mathrm{d}\varepsilon_2/2) \\ & +(-\zeta^2\cos(\alpha)^2 + \chi^2\sin(\alpha)^2)\sin(\mathrm{d}\varepsilon_1/2) \\ & \cos(\mathrm{d}\varepsilon_2/2))\sin(\Delta\phi) + (-\zeta^2\cos(\alpha)\sin(\beta) \\ & +\chi^2\sin(\alpha)\cos(\beta))\cos(\mathrm{d}\varepsilon_1/2 + \mathrm{d}\varepsilon_2/2)\cos(\Delta\phi) \end{aligned} \tag{A.6}$$

$$\begin{aligned} F = {} & \zeta\chi(\cos(\beta)\sin(\beta)\cos(\mathrm{d}\varepsilon_1/2)\sin(\mathrm{d}\varepsilon_2/2)\sin(2\Delta\phi) \\ & +\cos(\alpha)\cos(\beta)(\cos(\mathrm{d}\varepsilon_1/2)\cos(\mathrm{d}\varepsilon_2/2) \\ & -\sin(\mathrm{d}\varepsilon_1/2)\sin(\mathrm{d}\varepsilon_2/2)\cos(2\Delta\phi)) \\ & +\sin(\alpha)\sin(\beta)(-\sin(\mathrm{d}\varepsilon_1/2)\sin(\mathrm{d}\varepsilon_2/2) \\ & +\cos(\mathrm{d}\varepsilon_1/2)\cos(\mathrm{d}\varepsilon_2/2)\cos(2\Delta\phi)) \\ & +\sin(\alpha)\cos(\alpha)\sin(\mathrm{d}\varepsilon_1/2)\cos(\mathrm{d}\varepsilon_2/2)\sin(2\Delta\phi)) \end{aligned} \tag{A.7}$$

In these equations, $\mathrm{d}\varepsilon_1$ and $\mathrm{d}\varepsilon_2$ are the ellipticities of the two coincident beams (ideally zero), α and β are the orientation of the two polarizations relative to the polarizing beam splitter axes, ζ and χ are the transmission coefficients for the polarizing beam splitter (ideally equal to one), and

$\Delta\phi = \frac{4\pi n \cdot \Delta l}{\lambda}$ is the phase change introduced by a given displacement, Δl (n is the refractive index for the propagating medium and λ is the wavelength) for a single pass configuration of the interferometer. Note that the two angles, α and β, together determine both non-orthogonality between the two polarizations and rotation of the polarization axes relative to the polarizing beam splitter. For orthogonal, but rotationally misaligned, beams $\beta = -\alpha$. When the beams are perfectly aligned with the PBS, $\alpha = \beta = 0$. In this study, the model is modified in order to introduce a term specifically for non-orthogonality. Therefore, β is expressed as $\beta = \alpha +$ (non-orthogonality error) $= \alpha + \beta_{\text{err}}$. The displacement error, Δl_{pe}, due to the periodic phase error (A.1) is provided in (A.8).

$$\Delta l_{pe} = \frac{\Delta\phi_{pe} \cdot \lambda}{4\pi n} \tag{A.8}$$

References

Bergamin A, Cavagnero G and Mana G 1992 Phase holonomy in optical interferometry *J. Mod. Opt.* **39** 2053–74

Cosijns S, Haitjema H and Schellekens P 2002 Modeling and verifying non-linearities in heterodyne displacement interferometry *Precis. Eng.* **26** 445–55

Cukier R, Levine H and Schuler K 1978 Nonlinear sensitivity analysis of multiparameter model systems *J. Comput. Phys.* **26** 1–42

Homma T and Saltelli A 1996 Importance measures in global sensitivity analysis of nonlinear models *Reliab. Eng. Syst. Saf.* **52** 1–17

Hou W and Wilkening G 1992 Investigation and compensation on nonlinearity of heterodyne interferometers *Precis. Eng.* **14** 91–8

Hou W and Zhao X 1994 Drift of nonlinearity in the heterodyne interferometers *Precis. Eng.* **16** 25–35

Kennedy J and Eberhart R 1998 Particle swarm optimization *Proc. of the IEEE Int. Conf. on Evolutionary Computation* (Piscataway, NJ: IEEE Press) pp 69–73

Quenelle R 1983 Nonlinearity in interferometric measurements *Hewlett-Packard J.* **34** 10

Rosenbluth A E and Bobroff N 1990 Optical sources on nonlinearity in heterodyne interferometers *Precis. Eng.* **12** 7–11

Saltelli A 2002 Sensitivity analysis for importance assessment *Risk Anal.* **22** 579–90

Saltelli A, Andres T and Campolongo F 2008 *Global Sensitivity Analysis A Primer* (Hoboken, NJ: Wiley)

Saltelli S, Tarantola S and Chan K 1999 Quantitative model independent method for global sensitivity analysis of model output *Technometrics* **41** 39–56

Schmitz T and Beckwith J 2002 An investigation of two unexplored periodic error sources in differential-path interferometry *Precis. Eng.* **27** 311–22

Schmitz T, Chu D and Houck L III 2006 First-order periodic error correction: validation for constant and non-constant velocities with variable error magnitudes *Meas. Sci. Technol.* **17** 3195–203

Schmitz T and Kim H 2007 Monte Carlo evaluation of periodic error uncertainty *Precis. Eng.* **21** 251–9

Sobol' I M 1993 Sensitivity analysis for non-linear mathematical models *Math. Model. Comp. Exp.* **1** 407–14

Sobol' I M 2001 Global sensitivity indices for nonlinear mathematical models and their Monte Carlo estimates *Math. Comput. Simul.* **55** 271–80

Stone J A and Howard L P 1998 A simple technique for observing periodic nonlinearities in Michelson interferometers *Precis. Eng.* **22** 220–32

Sutton C 1987 Non-linearity in length measurement using heterodyne laser Michelson interferometry *J. Phys. E: Sci. Instrum.* **20** 1290–2

Wu C M and Deslattes R 1998 Analytical modeling of the periodic nonlinearity in heterodyne interferometry *Appl. Opt.* **37** 6696–700

Wu C M and Su C S 1996 Nonlinearity in measurements of length by optical interferometry *Meas. Sci. Technol.* **7** 62–8